

Design and Fabrication of a Portable 1-DOF Robotic Device for Indentation Tests

Masoud Moeinzadeh^a, Sheyda Davaria^a, Farshid Najafi^{a*} and Mojtaba Haghighi^a

^a School of Mechanical Engineering, College of Engineering, University of Tehran, Tehran, Iran

ARTICLE INFO

Article history:

Received: 10 April 2017

Accepted: 25 September 2017

Keywords:

Robotic device

Abdominal indentation

Tissue modeling

Viscoelastic model

ABSTRACT

There are many tactile devices for indentation examinations to measure mechanical properties of tissue. The purpose of this paper is to develop a portable indentation robotic device to show its usability for measuring the mechanical properties of a healthy abdominal tissue. These measurements will help to develop suitable mathematical models representing abdominal tissue. A 1-DOF portable robotic device has been designed to be placed on the patient's body. The device presses sensor plate on the abdomen. Force and position sensors measure the indentation force and displacement, respectively. Due to tissue time-dependent behavior, linear viscoelastic models with three, five and seven parameters have been selected for mathematical modeling. Nonlinear Least Squares (NLS) method is adopted to fit viscoelastic models with experimental data obtained from stress relaxation tests. Using Finite Prediction Error (FPE) criterion, viscoelastic model with five parameters has been selected as the optimal model. The results of the present paper can be used in abdominal tissue simulators to facilitate teaching palpation examinations.

1. Introduction

Palpation is a physical examination where organs or areas of body are touched with fingers to determine their size, shape, consistency, and location [1]. This method has been applied for localization of abnormal tissue in prostate, breast and cervix [2]. Stiffness difference between the unhealthy and the surrounding tissues help physicians to detect tumors in organs [3]. The palpation procedure in which the mechanical properties of the soft tissue is measured is referred to as "indentation" in the present paper.

The idea of using robotic devices for soft tissue indentation has been the subject of interest in many fields [4-6]. Several robotic devices providing normal indentations have been developed to characterize soft tissue properties [7-21]. Carter et al. [9] developed a static compliant probe for ex-vivo experiments on pig and sheep liver, and developed a hand-held compliant probe for in-vivo experiments on human liver. Ottensmeyer et al. [10, 11] used two different indentation devices to measure the mechanical response of the tissue. The TeMpeST and VESPI devices were developed to examine the small-strain frequency response and large-strain time domain response of tissue, respectively. Samur et al. [12] developed a robotic indenter for minimally invasive measurement of soft tissue in abdominal region. The robotic

device includes a robotic arm for indentation, a long laparoscopic indenter and a force sensor for insertion into the abdominal region. Liu et al. used a force-sensitive wheeled probe for localization of tissue abnormalities [13, 14]. The authors demonstrated that the results can be used for identifying the approximate location, shape and size of the nodules [15, 16]. Egorov et al. [8] developed a vaginal tactile imager. The device consists of a tactile sensor array and a tilt sensor. The authors used the device for detecting abnormal tissues in vaginal walls. Tanaka et al. [18, 19] developed an active palpation system for detecting tumors in human prostate. The system consists of a sensor and a vibro-machine. The sensor is attached to the physician's finger-tip, and the vibro-machine is attached to the root of the finger. In a few studies, automation of palpation for finding inclusions has been the subject of interest. Kato et al. [22] developed an automatic palpation robot, WAPRO-4R, for clinical testing of breast cancer. The robot was able to palpate the breast by pushing and dragging the skin laterally while using the pressure sensors embedded in its fingers.

In particular, from measurement and tissue modeling point of view, the material properties of various tissues have been measured in-vitro/vivo for decades. In-vitro tests, a sample is removed from the body and experimental tests are performed. In contrast, in-vivo tests, the material properties of the tissues are measured in live animals. By removing samples from body, the

* Corresponding Author. Tel.: +98 2161114861; Fax: +98 982161114861; e-mail: farshid_najafi@ut.ac.ir

tissue's mechanical properties may change drastically due to the factors such as temperature, hydration and loss of blood pressure [3]. Knowing these issues, it is more desirable to measure the mechanical properties of the tissues in live animals within their body. Experimental results reveal that elastic models provide only a rough approximation of the tissue behavior, mainly due to tissue time-dependent behavior [23, 24]. Viscoelastic models are time-dependent, and considered as a suitable option for tissue modeling. Many studies have focused on measuring and modeling the mechanical properties of living tissues. Farshad et al. [25] investigated the material properties of the pig kidney with a four-parameter viscoelastic model based on uniaxial tension tests on in-vitro samples. Davis et al. [26] developed a two-dimensional mathematical model for the pig spleen tissue from uniform compression tests by using a large-area indenter. The results showed that the mechanical properties of the tissue could be modeled as a nonlinear elastic membrane with an exponential stress-strain law. Liu et al. [27] developed a nonlinear viscoelastic model to represent the material properties based on a stress relaxation test.

In these studies, only the mechanical properties of a single tissue have been investigated. However, to the best of our knowledge, none of the above mentioned studies have used indenting devices to measure and model the mechanical properties of the abdominal tissue. A combination of skin, fat, muscles and internal organs makes the mechanical behavior of the abdominal tissue an interesting topic for investigation. Therefore, the purpose of this paper is to develop a portable indentation robotic device to measure the mechanical properties of the healthy abdominal tissue. These measurements help to develop suitable mathematical models which best fit the measured data.

In this paper, the detailed design of the robotic indentation device is presented. The proposed design has a set of specifications which makes it suitable for abdominal indentation. The device has one degree of freedom (DOF) where a cable mechanism is used to move the sensor plate. Mechanical properties of tissue can be calculated by measuring the contact force and the tissue deflection while pressing the sensor plate against the abdominal tissue. Mathematical models, experimental procedure, and the identification algorithm for determining the mechanical properties are described in the following sections. Finally, a suitable viscoelastic model using model validation method has been selected

2. Material and Methods

2.1. System Design

2.1.1. Design Requirements

The following factors are considered in the design of the robotic device for abdominal indentation task.

1. The device should be portable that can be handled and manipulated by an operator, Therefore, the weight of the device should be lower than 1 kg.
2. The power train of the device should be back-drivable in a way that patient's involuntary motions such as breathing can push back the device end-point.
3. The end-point of the device should have a linear stroke as much as 35mm to perform shallow indentation tests.
4. The power train of the device should be backlash-free not to deteriorate the relationship between the position of the end-point

and the rotational motion of the actuator. This can adversely affect the force-displacement measurements.

5. The end-point of the device should be equipped with a force sensor to directly measure the contact force between the device end-point and the abdominal tissue.

2.1.2. Developing the Basic Structure of the Device

There are various mechanisms which convert the rotary motion of an electric motor into a linear motion of an end-point. Rack-and-pinion, ball-screw and cable mechanism are the candidates to do this task. Both rack-and-pinion and ball-screw mechanisms are heavier than cable mechanisms. Moreover, back-driveability of the device end-point can be disrupted if ball-screw mechanism is used. Additionally, the cable mechanism can be implemented to provide a backlash-free power train.

2.1.3. Abdominal Indentation Device

A 1-DOF robotic device has been designed to be placed on the patient's body. The device presses the sensor plate on the abdomen (Figure 1). The force and position sensors measure the indentation force and the displacement of the abdominal tissue, respectively. The device is portable and can be handled easily.



Figure 1. Basic design of tactile device: (a) sensor plate; (b) abdomen

The power train of the device includes a DC motor and a cable drive system. The rotational motion of the motor is converted into the sliding motion of the device end-point by the cable drive. The cable drive system consists of a driver pulley, guiding pulleys, tightening pulley, a miniature cable loop and a slider (Figure 2). Figure 3 represents the detailed path of the cable. One side of the cable is fixed to the slider and the other side moves freely through the slider. In order to form a backlash-free friction drive, the driver pulley is threaded and the cable is wrapped around the pulley. The two other ends of the cable are terminated on the tightening pulley.

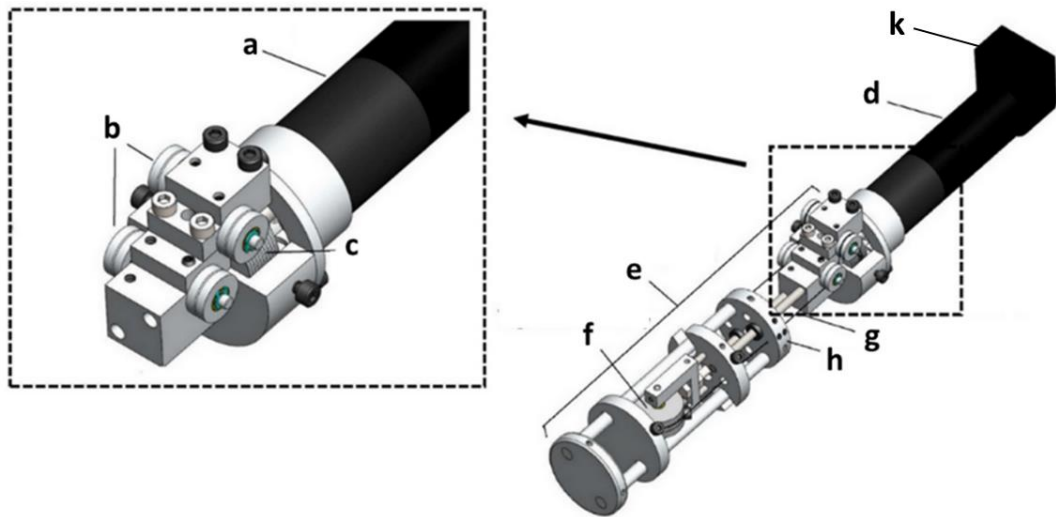


Figure 2. Power train of device: (a) gearbox; (b) guiding pulleys; (c) driver pulley; (d) DC motor; (e) cable drive system; (f) tightening pulleys; (g) miniature cable loop; (h) slider, (k) encoder

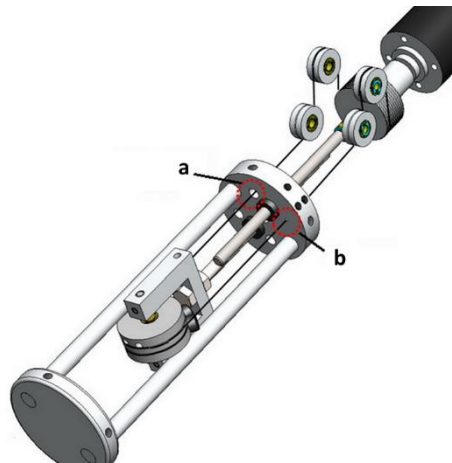


Figure 3. Detailed view of cable drive system: (a) moving free side; (b) fixed side

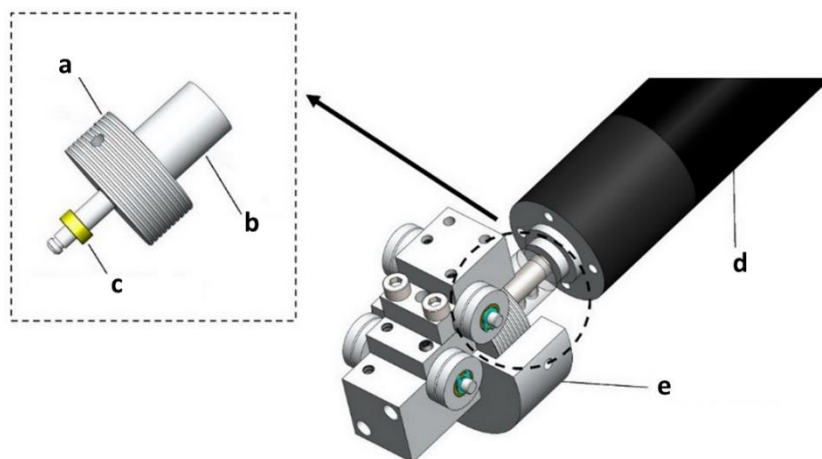


Figure 4. Driver pulley assembly in spool housing: (a) driver pulley; (b) spool shaft; (c) miniature ball bearing; (d) DC motor; (e) spool housing

The driver pulley is fixed to the shaft of the gearbox and its rotational motion is decoupled from the spool housing by miniature ball bearings placed inside the housing (Figure 4). Therefore, the actuator can rotate the driver pulley and the cable

loop. In order to form a backlash-free friction drive, the driver pulley is threaded and the cable is wrapped around the pulley (Figure 4). Two or three wrap can prevent the cable from slippage

on the pulley since the ratio of the high to low tension sides increases exponentially with the cable wrap angle.

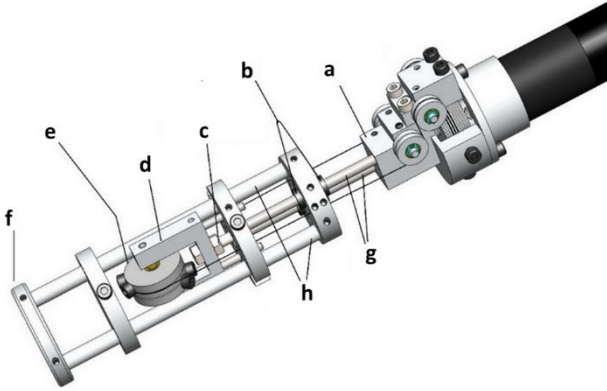


Figure 5. Inner parts of device: (a) pulley block; (b) linear ball bearing; (c) nut and bolt mechanism; (d) tightening; (e) tightening pulley; (f) sensor plate; (g) guiding rods; (h) pushing rods

In order to provide a low friction movement for the slider, linear ball bearings are used (Figure 5). Guiding rods are connected to the pulley block from one end and to the tightening plate from the other end. The slider's stroke is 50 mm which makes the device appropriate for performing abdominal indentation. Slider's linear motion is transferred to the sensor plate by pushing rods to generate the indentation motion of the device. The distance between the driver and tightening pulleys adjusts the tension in the cable by using the nut and bolt mechanism (Figure 5).

2.1.4. Force and Torque Relations

The relationship between torques and positions of the power train is shown in (Figure 6). Motor torque and angular position, τ_m and θ_m , are converted into output force and sensor plate position, F and r , respectively.

$$\tau_m = F \frac{d_p}{2N\eta} \quad (1)$$

$$r = d_p \frac{\theta_m}{2} \quad (2)$$

where d_p , N and η are driver pulley diameter, gearbox ratio and gearbox efficiency, respectively. In the present design, in order to create a frictional connection between driver pulley and the cable, the cable is wrapped a few times around the driver pulley connected to the motor shaft. Friction increases exponentially with the cable wrap angle according to the following equation.

$$\frac{T_1}{T_2} = e^{\mu\gamma_r} \quad (3)$$

Where T_1 is the high tension side, T_2 is the low tension side, μ is the coefficient of friction and γ_r is the cable wrap angle. Whereas, the tangential frictional force is proportional to the normal force multiplied by the coefficient of friction μ . The Eq. (3) holds for the case of impending slip. To prevent one side of the cable from slacking, cable pretension is required. To ensure that the cable does not slip, two ends of the cable are terminated on the driven pulley [28]. The motor torque and tension of the cable are related as follows:

$$\tau_m = 0.5 d_p (T_1 - T_2) \quad (4)$$

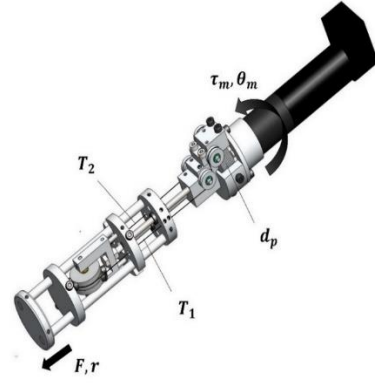


Figure 6. Forces and torques in cable drive system

2.1.5. Device Prototype

Figure 7 shows the prototype of the device. A Maxon permanent magnet DC motor (Maxon RE 25, 10 Watt) with a planetary gearhead (GP26B, reduction ratio: 4.4:1) has been selected as the device actuator. During the experiments, the maximum force exerted on the tissue is recorded as 9 N [29]. In the present design, driver pulley diameter, d_p , gearbox ratio, N , gearbox efficiency, η and the maximum recorded force, F , are 22 mm, 4.4, 0.84, and 9 N, respectively. Using Eq. (1) and the selected parameters, output motor torque, τ_m , is 26.7 mN.m which is lower than the continuous torque of the selected motor. The motor is equipped with an encoder (HEDL 5540, 500 CPT). Eq. (2) describes the relationship between the motor rotation/ encoder data, θ_m , and the sensor plate position, r . In order to measure the contact force between the sensor and the abdominal tissue during the indentation, a piezoresistive-based force sensor (Honeywell FS03) has been used. The maximum measurable force for the force sensor is 15 N. The device weight and dimensions are 600 gr and 270×40 mm, respectively, which makes it suitable as a portable indentation device.

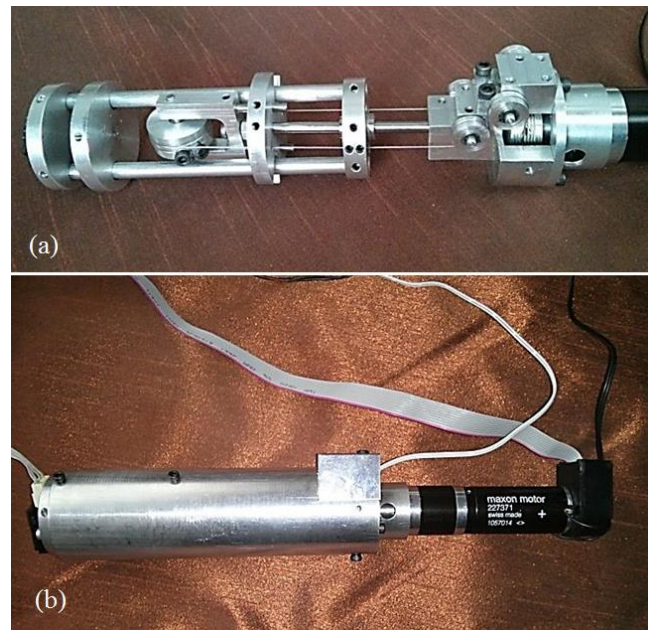


Figure 7. Prototyped device: (a) mechanism prototype; (b) device with cover

2.1.6. Device Calibration

For calibrating the encoder, the distance travelled by the tip of the device was measured by a caliper, and was compared with the number of output pulses of the encoder. For force sensor calibration, the output voltage of the force sensor is measured when 0.2, 0.5 and 1 kg standard loads are applied to the sensor. The output voltage of the force sensor is amplified by an op-amp where the offset voltage of the op-amp is eliminated by using a potentiometer.

2.2. Tissue Modeling

In this section, the capability of the indentation device in conducting experiments on human abdomen is demonstrated as a proof-of-concept rather than a source for precise values of tissue properties.

2.2.1. Viscoelastic Modelling

A viscoelastic material exhibits both elastic solid-like, and viscous fluid-like behaviors, which are modeled by a spring and dashpot, respectively. These materials continue to deform when they are under a constant force (creep) and continue to relax when they are under a constant displacement (stress relaxation). They exhibit hysteresis when they are under cyclic load where the loading phase is different from the unloading one [30].

The mechanical behavior of the biological soft tissue is time-dependent and nonlinear. A full description of the mechanical response of the soft tissue to loads requires a nonlinear viscoelastic model, which is built on a firm theoretical and physical foundation. Existing models require a large number of material constants [31]. Nonlinear springs and dashpots can be used for models representing the nonlinear viscoelastic properties of the materials such as soft tissues. However, nonlinear viscoelastic models are used whenever stress/strain lies in the nonlinear region of viscoelasticity. On the other hand, linear models can readily model the material behavior when stress/strain lies in the linear viscoelastic region. In this study, the level of stress or strain is low and linear models can therefore be employed [32].

A model that predicts the time-dependent behavior of the soft tissue from a simple experiment is needed; preferably, the terms in the model should be few in number and should not be time-dependent so that they can be easily obtained. Linear viscoelastic models are presented in different order. Increasing the complexity (order) of the model causes a better prediction of the behavior of the soft tissue in cost of computational load [24]. The Standard Linear Solid (SLS) model, as shown in Figure 8, is the simplest model that has both creep and stress relaxation response which resemble real materials. In this model, a linear spring, E_1 , and a linear dashpot, μ_1 , are connected in series and another linear spring, E_0 , is connected in parallel [24]. In this paper, the SLS model is called three-element model, where three unknown parameters needed to be calculated.

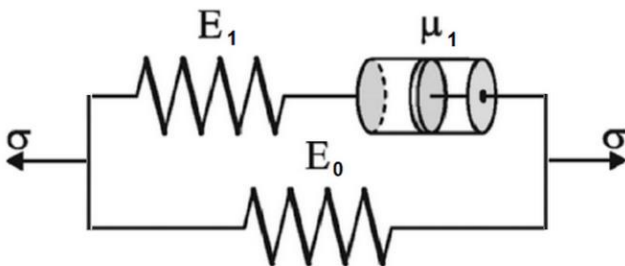


Figure 8. Maxwell form of SLS model

For consistency with the rest of other research papers [33-35], higher order models are considered with addition of linear springs and linear dashpots. A linear spring-dashpot, in series, should be added to the lower order model, in parallel, which creates Double Maxwell-arm Wichert (DMW) and Triple Maxwell-arm Wichert (TMW) models (Figure 9) [24]. In this paper, the SLS, DMW and TMW models are evaluated to find out which model represents the abdominal behavior in indentation tests, properly.

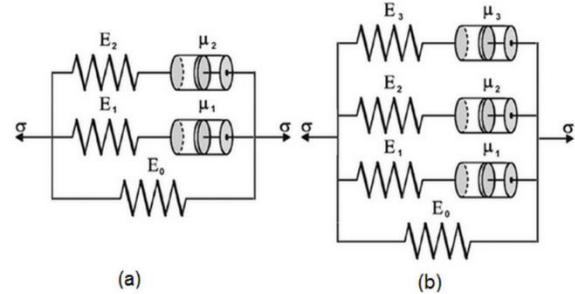


Figure 9. (a) Double Maxwell-arm Wichert (DMW) model; (b) Triple Maxwell-arm Wichert (TMW) model

2.2.2. Mathematical Model of Indentation Test

Analytical equations for characterization of tissue under indentation are desirable. The analytical equation describing the total normal load needed to indent to a specific depth on a viscoelastic sample test material, here is abdomen, is given as Eq. (5) [24]. In this paper, the test materials are assumed to be incompressible, since most living tissues can be considered as incompressible material under indentation [24]. Therefore, the Poisson's ratio, ν is considered as 0.5.

$$F(t) = \frac{2\Omega R d}{1 - \nu^2} E_v(t) = \frac{8R\Omega d}{3} E_v(t) \tag{5}$$

where $F(t) N$ denotes the compression force, and $E_v(t) N/m^2$ expresses the relaxation modulus and depends on the order of the model. $R = 0.002 m$ and $d = 0.015 m$ are the radius of the indentation tip, and the indentation depth, respectively. Ω can be written as [24]:

$$\Omega = (1 + 1.33p + 1.283p^2 + 0.769p^3 + 0.0975p^4) \tag{6}$$

where $p = \frac{\sqrt{Rd}}{h}$ and h in meters denotes the thickness of the material. For SLS model, the equation for the relaxation modulus, E_v is:

$$E_v(t) = E_0 + E_1 e^{-\frac{t}{\tau_1}} \tag{7}$$

Where t in Eq.(7) is in seconds, and τ_1 is called relaxation time constant in seconds. In linear viscoelastic models, τ can be related to the decaying time of the mechanical response of the material. Large relaxation times are related to slowly decaying responses or small applied strain rates. Small relaxation times are related to fast decaying responses or high applied strain rates. In a phenomenological sense, this time constant may be thought of as characteristic relaxation time of the material. The relaxation modulus for the DMW and TMW models can be written as follows. For the DMW model we have:

$$E_v(t) = E_0 + E_1 e^{-\frac{t}{\tau_1}} + E_2 e^{-\frac{t}{\tau_2}} \tag{8}$$

And for the TMW model we have [32]:

$$E_v(t) = E_0 + E_1 e^{-\frac{t}{\tau_1}} + E_2 e^{-\frac{t}{\tau_2}} + E_3 e^{-\frac{t}{\tau_3}} \quad (9)$$

2.3. Experimental Method

2.3.1. Indentation Test Setup and Procedure

The experimental setup is illustrated in Figure 10 which includes the indentation device, interface board, a power supply, and a laptop. Indentation test was done on the left lumbar region of the abdomen using the proposed device (Figure 11). In order to perform the indentation, the tactile device must be tangent to the surface of the abdomen where h is selected as 0.025 m. Immediately after the initial contact, the tip started to indent a given depth, $d = 1.5$ cm, into the abdomen at a relatively high velocity, $V = 1$ cm/s, to simulate the step input without causing vibration in the test region. After reaching the desired depth, the position of the indentation tip was fixed for a given amount of time, $t = 350$ s, necessary for the force relaxation data approaching a final steady state value. In the current work, tissue viscoelastic parameters are calculated using relaxation tests.

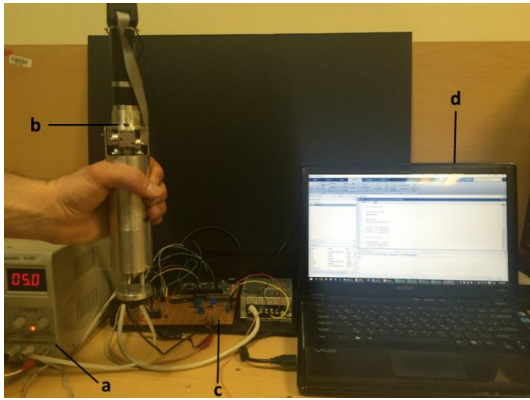


Figure 10. Experimental setup: (a) power supply; (b) palpation device; (c) control board; (d) laptop



Figure 11. Human's abdomen under indentation test using prototype device

3. Results

3.1. Indentation Results

A total number of three trials were performed. Figure 12 shows the load-time curve of a sample trial. Fluctuations caused by human respiratory motions are observed in the output data. Due to the dominant influence of respiration in load-time data, calculating the mechanical properties of the test point is almost impossible. Therefore, it is necessary to obtain the respiration load-time cycle in order to remove the effect of this factor. With reference to Figure 12, the downward slope of the data, clearly visible in the

early moments of the test, reaches a steady state condition, with some fluctuations due to the respiration, after about 300 seconds. Hence, another indentation test with the same condition was done for extracting the full cycle of load-time curve of breathing. In this test, after indenting to the desired depth, data collection starts after seven minutes and lasts for twenty seconds (Figure 13). The seven minutes delay in data collection is to ensure greater accuracy and higher reliability in reaching the steady state condition.

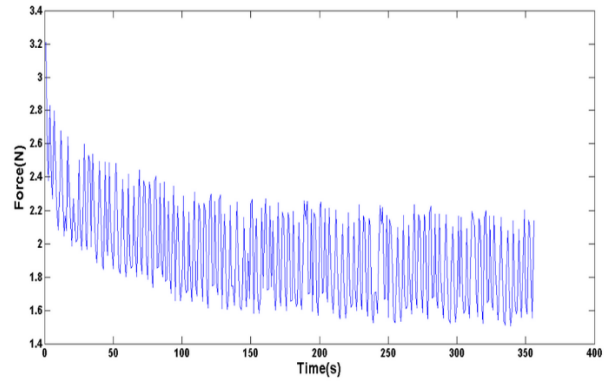


Figure 12. Indentation results with breathing effect

The amount of force is influenced by two factors: i) the average value that reaches to 1.8N following the first 5 minutes of the test (Figure 12), and is due to the indentation effect; ii) respiration which causes fluctuations in data. By subtracting the average value of the indentation force from data points in the range of 420 to 440 seconds, the data of Figure 13 have been achieved. Figure 13, therefore, clearly shows the full cycles of breathing in the range of the study. These cycles are similar to sine waves with amplitude of 0.3 N and time-period of 4 seconds. Next, an algorithm was written in MATLAB where the corresponding upper and lower values of cycle were averaged in order to remove the effect of respiration. Figure 14 shows the new load-time curves of three relaxation tests on left lumbar region with using the above mentioned algorithm. Therefore, these sets of new data are used for further analysis in the present study. Mechanical properties of abdominal region under indentation are extracted with the approach of the relaxation test for viscoelastic materials.

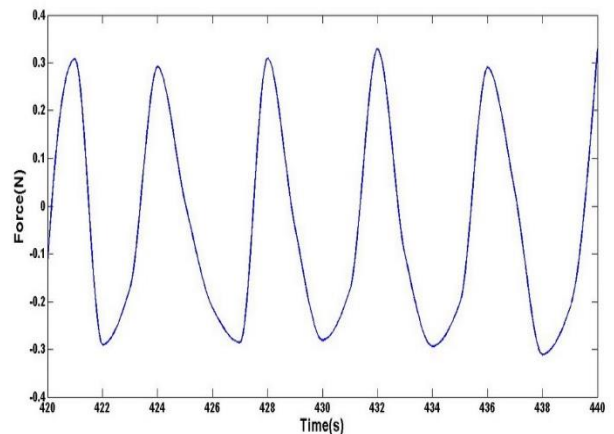


Figure 13. Breathing cycle

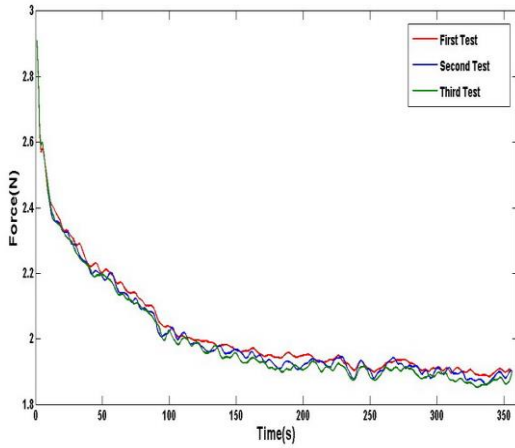


Figure 14. Indentation by removing the effect of breathing

3.2. Identification Algorithm

A MATLAB program was developed to fit Eq. (5) to the stress relaxation load–time, curve obtained from the experimental data, using NLS curve fitting method. The values of the estimated parameters in E_v depend on the experimental data and the viscoelastic model.

3.3. Model Estimation

Viscoelastic model, experimental data, and NLS curve-fitting method are used to identify model parameters with different orders. Estimated parameters of viscoelastic models are presented in Table 1-3. Figure 15 shows the comparison of the mean value of the three experimental data fitted with the three viscoelastic models. Improvement of the fitting is observed from SLS model to DMW and TMW models.

Table 1. Estimated parameters of SLS model

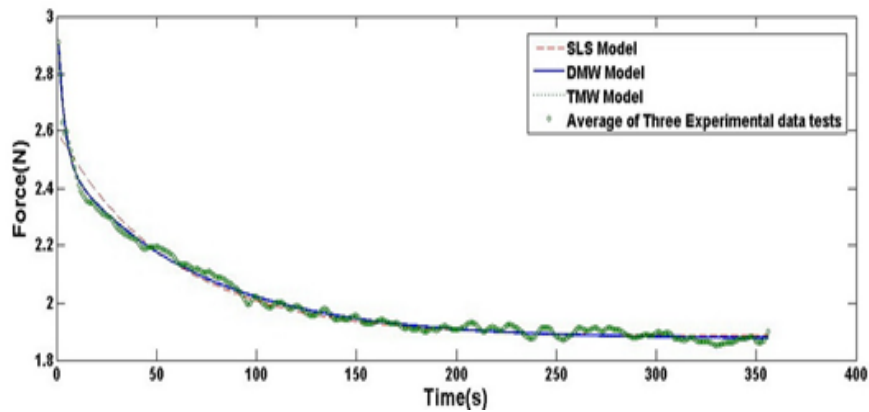
SLS Model	E_0 (kPa)	E_1 (kPa)	τ_1 (s)	R-squared	Sum of Squared Errors (SSE)
First test	8.25	2.97	59.9	0.8908	5.30e6
Second Test	8.20	3.00	57.8	0.8868	5.61e6
Third test	8.14	3.11	56.7	0.8927	5.33e6
Mean	8.19	3.02	58.1	0.8901	5.41e6

Table 2. Estimated parameters of DMW model

SLS Model	E_0 (kPa)	E_1 (kPa)	E_2 (kPa)	τ_1 (s)	τ_2 (s)	R-squared	Sum of Squared Errors (SSE)
First test	8.21	2.61	2.51	71.7	2.8	0.9330	1.20e6
Second Test	8.15	2.62	2.51	70.3	3.0	0.9324	1.29e6
Third test	8.10	2.72	2.35	68.5	3.2	0.9333	1.26e6
Mean	8.15	2.65	2.46	70.16	3	0.9329	1.25e6

Table 3. Estimated parameters of TMW model

SLS Model	E_0 (kPa)	E_1 (kPa)	E_1 (kPa)	E_1 (kPa)	τ_1 (s)	τ_2 (s)	τ_3 (s)	R-squared	Sum of Squared Errors (SSE)
First test	8.2	2.6	1.68	1.57	72	3.7	1	0.9542	1.18e6
Second Test	8.15	2.61	1.71	1.48	70.7	3.8	.95	0.9203	1.32e6
Third test	8.10	2.70	1.64	1.53	69.2	4	0.97	0.9431	1.22e6
Mean	8.15	2.63	1.67	1.52	70.6	3.8	0.97	0.9392	1.24e6



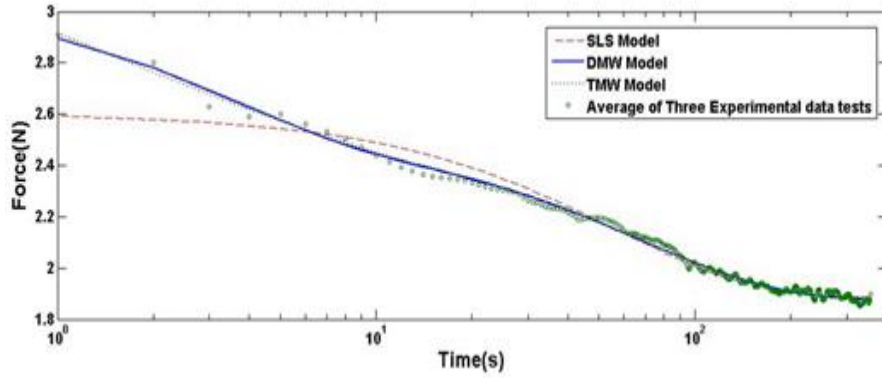


Figure 15. Averaged of three indentation tests on left lumbar region of the abdomen fitted with the SLS, DMW and TMW models in normal and logarithmic scales

Figure 15 shows the result of fitting Eq. (5) to the results obtained from the first trial of the indentation tests. With reference to Figure 15, the SLS model has already been shown to be incapable of precisely capturing the properties of biological tissue. A comparison of R-squared values for the SLS, DMW and TMW models in Tables 1 to 3 show an increasing trend. The increase is more pronounced when DMW and TMW models are used instead of SLS model. The difference in R-squared values of DMW and TMW models is not significant. This limited improvement with the TMW model was actually achieved at the cost of introducing another two independent parameters, causing computational difficulties in numerical modeling. In the next section, the appropriate model selection for our experiments will be discussed with another approach.

3.4. Model Validation and Selection

To validate the estimated model, residual signal $\epsilon(t)$ is used. NLS curve fitting method selects best model parameters that minimize sum of squared residuals. The minimized value depends on the order of the model and the number of data in each experiment. FPE criteria is used for model validation, and the best model with mathematical simplicity and fitting accuracy has been selected. Mathematical formulation for LSE cost function is [36]:

$$V_N = \frac{1}{2} \sum_{i=1}^N \epsilon(i)^2 = \frac{1}{2} \times RSS \tag{10}$$

$$\epsilon(t) = y(t) - \hat{y}(t) \tag{11}$$

where $y(t)$ and $\hat{y}(t)$ are experimental data output, reaction load of abdomen, and estimated output by viscoelastic model, respectively. $\epsilon(t)$ is the residual, and N is the number of the data points. Mathematical formulation for the FPE criteria is [36]:

$$W_N^{FPE} = V_N \frac{1 + p/N}{1 - p/N} \tag{12}$$

where p , N , V_N are the number of the parameters, the number of data in each experiment and the minimum value of the cost function, respectively. For instance, the value of p in the SLS model is three.

The result of the comparisons is summarized in Table 4. Finally, the five-parameter model (TMW) with minimum W_N^{FPE} is selected which satisfactorily represents the experimental results. This model has mathematical simplicity and fitting accuracy based on FPE criteria.

Table 4. Comparison between model orders using FPE criteria

Model Order	Optimal value of LSE cost function ($V_N(\hat{\theta}_N)$)	Number of parameters (p)	Value of w in FPE test (W_N^{FPE})	Mean of residual	Variance of residuals
3(SLS)	2.7e6	3	5.50e6	6.21e-5	8.041e-4
5(DMW)	6.25e5	5	6.40e5	6.11e-7	1.89e-4
7(TMW)	6.20e5	7	6.45e5	6.06e-7	1.84e-4

4. Discussion

The purpose of this paper is to show the practicality of the indentation device for performing the experiments on the human abdomen and representing a simple mechanical response model. During the indentation test, the sensor plate touches the tissue and the force sensor measures the interaction forces. The deflection of the tissue is measured by a position sensor.

The response behavior of the abdominal tissue is modeled by linear viscoelastic relationships based on relaxation tests. The accurate region of the reported relaxation function is bounded by

the long time limits of the step relaxation test [37]. The long time limit of the relaxation time is chosen based on the response of the abdominal region. For modeling with higher accuracy, the response should be reached to a steady state condition. To select appropriate linear viscoelastic model, a procedure is used which starts from a basic viscoelastic model with three-parameters, and increases model order until the best model is achieved. Numerical computations show that a five-order linear viscoelastic model is the optimal one. Therefore, with model validation methods, such as FPE criteria, the optimal model with mathematical simplicity and accuracy can be achieved.

Finally, certain precautions have been adopted to minimize the effect of nonlinearity in the testing configuration, such as limiting the indentation depth to less than 10% of the sample thickness. The extension of the current study to include non-linear viscoelastic models with different loading conditions and larger stress/strain is in progress in this research group.

5. Acknowledgment

The authors would like to thank the Iran National Science Foundation (INSF) who provided financial support for this research.

6. Appendix

6.1. R-squared

The coefficient of determination, R-squared, is the proportion of the variance in the dependent variable that is predictable from the independent variable. The R-squared for a linear regression model with one independent variable is:

$$R\text{-squared} = \frac{SSR}{SST} \quad (1)$$

where

$$SSR = \sum_i (\hat{y}_i - \bar{y})^2 \quad (2)$$

and:

$$SST = \sum_i (y_i - \bar{y})^2 \quad (3)$$

Where y_i and \hat{y}_i and \bar{y} are the original data values, modeled values and averaged values, respectively. SST is the total sum of squares and SSR is the regression sum of squares. The range of R-squared is from 0 to 1. An R-square of 0 shows that the dependent variable cannot be predicted from the independent variable and an R-square of 1 shows that the dependent variable can be predicted without error from the independent variable [41].

6.2. Sum of Squared Residuals (SSE)

SSE quantifies how much the original data points, y_i , vary around the modeled data values, \hat{y}_i . SSE can be defined as:

$$SST = \sum_i (\hat{y}_i - \hat{y})^2 \quad (4)$$

It should be noted that $SST = SSR + SSE$ [41].

References

[1] S. Ullrich, T. Kuhlen, Haptic palpation for medical simulation in virtual environments, *Visualization and Computer Graphics*, IEEE Transactions on, Vol. 18, No. 4, pp. 617-625, 2012.
 [2] S. E. Waggoner, Cervical cancer, *The Lancet*, Vol. 361, No. 9376, pp. 2217-2225, 2003.
 [3] J. Kim, B. Ahn, S. De, M. A. Srinivasan, An efficient soft tissue characterization algorithm from in vivo indentation experiments for medical simulation, *The international journal of medical robotics and computer assisted surgery*, Vol. 4, No. 3, pp. 277-285, 2008.
 [4] P. Dario, M. Bergamasco, An advanced robot system for automated diagnostic tasks through palpation, *Biomedical Engineering*, IEEE Transactions on, Vol. 35, No. 2, pp. 118-126, 1988.
 [5] A. Bicchi, G. Canepa, D. D. Rossi, P. Iacconi, E. P. Scilingo, A sensor-based minimally invasive surgery tool for detecting tissue elastic properties, in *Proceeding of, IEEE*, pp. 884-888.

[6] E. Scilingo, D. DeRossi, A. Bicchi, P. Iacconi, Haptic display for replication of rheological behavior of surgical tissues: modelling, control, and experiments, in *Proceeding of*.
 [7] J. Yan, P. K. Scott, R. S. Fearing, Inclusion probing: signal detection and haptic playback of 2D FEM and experimental data, in *Proceeding of*, 14-19.
 [8] V. Egorov, H. Van Raalte, A. P. Sarvazyan, Vaginal tactile imaging, *Biomedical Engineering*, IEEE Transactions on, Vol. 57, No. 7, pp. 1736-1744, 2010.
 [9] F. J. Carter, T. G. Frank, P. J. Davies, D. McLean, A. Cuschieri, Measurements and modelling of the compliance of human and porcine organs, *Medical Image Analysis*, Vol. 5, No. 4, pp. 231-236, 2001.
 [10] M. P. Ottensmeyer, Minimally invasive instrument for in vivo measurement of solid organ mechanical impedance, Thesis, Massachusetts Institute of Technology, 2001.
 [11] M. P. Ottensmeyer, A. E. Kerdok, R. D. Howe, S. L. Dawson, The effects of testing environment on the viscoelastic properties of soft tissues, in: *Medical Simulation*, Eds., pp. 9-18: Springer, 2004.
 [12] E. Samur, M. Sedef, C. Basdogan, L. Avtan, O. Duzgun, A robotic indenter for minimally invasive measurement and characterization of soft tissue response, *Medical Image Analysis*, Vol. 11, No. 4, pp. 361-373, 2007.
 [13] H. Liu, D. P. Noonan, K. Althoefer, L. D. Seneviratne, Rolling mechanical imaging: a novel approach for soft tissue modelling and identification during minimally invasive surgery, in *Proceeding of, IEEE*, pp. 845-850.
 [14] H. Liu, D. P. Noonan, B. J. Challacombe, P. Dasgupta, L. D. Seneviratne, K. Althoefer, Rolling mechanical imaging for tissue abnormality localization during minimally invasive surgery, *Biomedical Engineering*, IEEE Transactions on, Vol. 57, No. 2, pp. 404-414, 2010.
 [15] K. Sangpradit, H. Liu, L. D. Seneviratne, K. Althoefer, Tissue identification using inverse finite element analysis of rolling indentation, in *Proceeding of, IEEE*, pp. 1250-1255.
 [16] K. Sangpradit, H. Liu, P. Dasgupta, K. Althoefer, L. D. Seneviratne, Finite-element modeling of soft tissue rolling indentation, *Biomedical Engineering*, IEEE Transactions on, Vol. 58, No. 12, pp. 3319-3327, 2011.
 [17] P.-L. Yen, D.-R. Chen, K.-T. Yeh, P.-Y. Chu, Lateral exploration strategy for differentiating the stiffness ratio of an inclusion in soft tissue, *Medical engineering & physics*, Vol. 30, No. 8, pp. 1013-1019, 2008.
 [18] S. Chonan, Z. W. Jiang, M. Tanaka, T. Kato, M. Kamei, Y. Tanahashi, Development of a palpation sensor for detection of prostatic cancer and hypertrophy (optimum structural design of sensor), *International Journal of Applied Electromagnetics and Mechanics*, Vol. 9, No. 1, pp. 25-38, 1998.
 [19] M. Tanaka, H. Nesori, Y. Tanahashi, Development of an active palpation sensor wearable on a finger for detecting prostate cancer and hypertrophy, *Ann of NanoBME*, Vol. 1, pp. 141-147, 2008.
 [20] L. Han, A. Noble, M. Burcher, The elastic reconstruction of soft tissues, in *Proceeding of, IEEE*, pp. 1035-1038.
 [21] J. Kim, M. A. Srinivasan, Characterization of viscoelastic soft tissue properties from in vivo animal experiments and inverse FE parameter estimation, in: *Medical Image Computing and Computer-Assisted Intervention—MICCAI 2005*, Eds., pp. 599-606: Springer, 2005.
 [22] I. Kato, K. Koganezawa, A. Takanishi, Automatic breast cancer palpation robot: WAPRO-4, *Advanced Robotics*, Vol. 3, No. 4, pp. 251-261, 1988.
 [23] T. P. Prevost, A. Balakrishnan, S. Suresh, S. Socrate, Biomechanics of brain tissue, *Acta biomaterialia*, Vol. 7, No. 1, pp. 83-95, 2011.
 [24] X. Wang, J. A. Schoen, M. E. Rentschler, A quantitative comparison of soft tissue compressive viscoelastic model accuracy, *Journal of the mechanical behavior of biomedical materials*, Vol. 20, pp. 126-136, 2013.
 [25] M. Farshad, M. Barbezat, P. Flüeler, F. Schmidlin, P. Graber, P. Niederer, Material characterization of the pig kidney in relation with the biomechanical analysis of renal trauma, *Journal of Biomechanics*, Vol. 32, No. 4, pp. 417-425, 1999.
 [26] P. J. Davies, F. J. Carter, D. G. Roxburgh, A. Cuschieri, Mathematical Modelling for Keyhole Surgery Simulations: Spleen Capsule as an Elastic Membrane, *Computational and Mathematical Methods in Medicine*, Vol. 1, No. 4, pp. 247-262, 1999.
 [27] H. Liu, D. P. Noonan, Y. H. Zweiri, K. Althoefer, L. D. Seneviratne, The development of nonlinear viscoelastic model for the application of soft tissue identification, in *Proceeding of, IEEE*, pp. 208-213.
 [28] A. J. Madhani, Design of teleoperated surgical instruments for minimally invasive surgery, PHD Thesis, MIT, 1998.
 [29] E. Karadogan, R. L. Williams, J. N. Howell, R. R. Conatser Jr, A stiffness discrimination experiment including analysis of palpation forces and velocities, *Simulation in Healthcare*, Vol. 5, No. 5, pp. 279-288, 2010.

- [30] A. E. Kerdok, Characterizing the nonlinear mechanical response of liver to surgical manipulation, Thesis, Harvard University Cambridge, MA, 2006.
- [31] H. W. Haslach, Nonlinear viscoelastic, thermodynamically consistent, models for biological soft tissue, *Biomechanics and Modeling in Mechanobiology*, Vol. 3, No. 3, pp. 172-189, 2005.
- [32] H. F. Brinson, L. C. Brinson, Polymer engineering science and viscoelasticity, in: Eds., pp. 172, Berlin: Springer, 2008.
- [33] M. Sedef, E. Samur, C. Basdogan, Real-time finite-element simulation of linear viscoelastic tissue behavior based on experimental data, *IEEE Computer Graphics and Applications*, Vol. 26, No. 6, 2006.
- [34] E. Clayton, J. Garbow, P. Bayly, Frequency-dependent viscoelastic parameters of mouse brain tissue estimated by MR elastography, *Physics in medicine and biology*, Vol. 56, No. 8, pp. 2391, 2011.
- [35] M. Caputo, J. M. Carcione, F. Cavallini, Wave simulation in biologic media based on the Kelvin-Voigt fractional-derivative stress-strain relation, *Ultrasound in medicine & biology*, Vol. 37, No. 6, pp. 996-1004, 2011.
- [36] T. Söderström, P. Stoica, 1988, System identification, Prentice-Hall, Inc.,
- [37] J. Funk, G. Hall, J. Crandall, W. Pilkey, Linear and quasi-linear viscoelastic characterization of ankle ligaments, *Journal of biomechanical engineering*, Vol. 122, No. 1, pp. 15-22, 2000.
- [38] Y.-C. Fung, Stress-strain-history relations of soft tissues in simple elongation, *Biomechanics: Its foundations and objectives*, Vol. 7, pp. 181-208, 1972.
- [39] A. Nekouzadeh, G. M. Genin, Adaptive quasi-linear viscoelastic modeling, in: *Computational Modeling in Tissue Engineering*, Eds., pp. 47-83: Springer, 2012.
- [40] R. De Pascalis, I. D. Abrahams, W. J. Parnell, On nonlinear viscoelastic deformations: a reappraisal of Fung's quasi-linear viscoelastic model, in *Proceeding of, The Royal Society*, pp. 20140058.
- [41] A. Papoulis, S. U. Pillai, 2002, Probability, random variables, and stochastic processes, Tata McGraw-Hill Education.